Controls on the strength and structure of the Atlantic meridional overturning circulation in climate models

Manali S. Nayak[1,2,*], David B. Bonan[3,*], Emily R. Newsom[3], Andrew F. Thompson[3]

[1]Department of Physics, The Ohio State University, Columbus, OH, USA
[2]Department of Atmospheric Sciences, University of Washington, Seattle, WA, USA
[3]Environmental Science and Engineering, California Institute of Technology, Pasadena, CA, USA
[*]These authors contributed equally to this work.

Key Points:

- The thermal-wind expression captures the intermodel spread in mean-state AMOC strength across climate models.
- Intermodel variations in the AMOC strength are related to intermodel variations in the overturning scale depth.
- Climate models with a stronger AMOC exhibit a larger scale depth, and larger North Atlantic surface buoyancy loss and weaker stratification.

Corresponding author: Manali Nayak; David Bonan, `manalin@uw.edu`; `dbonan@caltech.edu`

Abstract

State-of-the-art climate models simulate a large spread in the mean-state Atlantic meridional overturning circulation (AMOC), with strengths varying between 12 and 25 Sv. Here, we introduce a framework for understanding this spread by assessing the balance between the thermal-wind expression and surface water mass transformation in the North Atlantic. The intermodel spread in the mean-state AMOC strength is shown to be related to the overturning scale depth: climate models with a larger scale depth tend to have a stronger AMOC. Intermodel variations in the overturning scale depth are also related to intermodel variations in North Atlantic surface buoyancy loss and stratification. We present a physically-motivated scaling relationship that links intermodel variations in the scale-depth to surface buoyancy fluxes and stratification in the North Atlantic, and thus connects North Atlantic surface processes to the interior ocean circulation. These results offer a framework for reducing mean-state AMOC biases in climate models.

Plain Language Summary

The Atlantic meridional overturning circulation – a branch of ocean currents confined to the Atlantic basin – strongly influences regional climate by redistributing heat, freshwater and carbon throughout the ocean. Understanding the processes that control the strength of this circulation feature, particularly in state-of-the-art climate models, remains an active area of research. In this study, we introduce a conceptual framework to understand the processes that contribute to a large spread in the strength of the Atlantic meridional overturning circulation across climate models. We find climate models that exhibit stronger circulation also have a deeper circulation. We introduce another expression to show that climate models with a deeper circulation also have stronger surface buoyancy loss and weaker stratification in the North Atlantic, which allows for more formation of dense waters that supply the southward flowing component of the Atlantic meridional overturning circulation. These results provide a framework for reducing biases in simulating the present-day Atlantic meridional overturning circulation in climate models.

1 Introduction

The ocean's global overturning circulation (GOC) is a complex system of currents that connects different ocean basins (Gordon, 1986; Broecker, 1991; Lumpkin & Speer, 2007; Talley, 2013). The branch of the GOC that is localized to the Atlantic basin, often referred to as the Atlantic meridional overturning circulation (AMOC), is a unique feature of the GOC because it transports heat northward at all latitudes (Ganachaud & Wunsch, 2003) and ventilates the upper 2000 m of the ocean (Buckley & Marshall, 2016). The AMOC plays a central role in modulating regional and global climate by impacting Atlantic sea-surface temperatures, which cause changes to the African and Indian monsoon, the summer climate over North America and Western Europe, and Arctic sea ice (Zhang & Delworth, 2006; Mahajan et al., 2011; Zhang et al., 2019). The AMOC is also thought to play a leading order role in setting the peak of tropical rainfall in the Northern Hemisphere (Frierson et al., 2013; Marshall et al., 2014). For these reasons, understanding what controls the strength and structure of the AMOC remains a central goal of climate science.

Despite decades of research on the AMOC, the intermodel spread in the mean-state AMOC strength across state-of-the-art global climate models (GCMs) remains large (e.g., Schmittner et al., 2005; Cheng et al., 2013; Reintges et al., 2017; Weijer et al., 2020; Jackson & Petit, 2023). For example, in pre-industrial control simulations from GCMs participating in Phase 6 of the Coupled Model Intercomparison Project (CMIP6), the mean-state AMOC strength, which is calculated as the maximum of the meridional overturning circulation in the Atlantic basin, varies between 12 and 25 Sv (1 Sv $\equiv 10^6$ m^3 s^{-1}; Fig. 1). GCMs also simulate a large intermodel spread in the AMOC strength at all depths. GCMs with a weaker maximum AMOC (e.g., IPSL-CM6A-LR) tend to exhibit a weaker AMOC throughout the upper cell, whereas those with a stronger maximum AMOC (e.g., NorESM2-MM) tend to exhibit a stronger AMOC throughout the upper cell (Fig. 1). There is also a close relationship between the strength and depth of the AMOC in GCMs: the depth of the maximum AMOC strength tends to be greater in GCMs with a stronger AMOC (compare circles in Fig. 1). The large intermodel spread in both the strength and structure of the mean-state AMOC leads to a key question: What causes the intermodel spread in the mean-state AMOC strength across GCMs? Given that the mean-state AMOC strength is linked to the magnitude of AMOC weakening under warming in GCMs (e.g., Gregory et al., 2005; Winton et al., 2014; Weijer et al., 2020; Baker et al., 2023), a better understanding of mean-state AMOC processes may improve future climate projections.

Historically, variations in the AMOC strength have been attributed to processes affecting surface buoyancy fluxes in the North Atlantic, as this is where North Atlantic Deep Water (NADW) forms (e.g., Klinger & Marotzke, 1999; Marotzke & Klinger, 2000; Samelson, 2009; Wolfe & Cessi, 2011; Radko & Kamenkovich, 2011; Sévellec & Fedorov, 2016; Wang et al., 2010; Heuzé, 2021; Lin et al., 2023; Jackson & Petit, 2023). For example, Lin et al. (2023) found that GCMs with a stronger mean-state AMOC tend to have a less stratified North Atlantic, which permits deeper open-ocean convection and thus stronger NADW formation. Studies have also related the AMOC strength to the meridional density difference between the low- and high-latitude regions of the Atlantic basin (Stommel, 1961; Hughes & Weaver, 1994; Thorpe et al., 2001). However, subsequent work showed that meridional density gradients do not control the AMOC strength (De Boer et al., 2010). Other work has argued that the Southern Ocean plays a primary role in setting the strength and structure of the AMOC through a combination of wind-driven Ekman transport and eddy transport (Toggweiler & Samuels, 1998; Gnanadesikan, 1999; Vallis, 2000; Wolfe & Cessi, 2010; De Boer et al., 2010; Sévellec & Fedorov, 2011; Wolfe & Cessi, 2011; Nikurashin & Vallis, 2012; Marshall et al., 2017; Saenko et al., 2018; Nadeau & Jansen, 2020), and surface buoyancy forcing (Shakespeare & Hogg, 2012; Ferrari et al., 2014; Jansen & Nadeau, 2016; Baker et al., 2020). Yet, the equilibrium AMOC strength in coupled GCMs has been shown to be relatively unchanged with strengthened winds over the Southern Ocean (Jochum & Eden, 2015; Gent, 2016), potentially due to compensating effects from eddy transport

(Abernathey et al., 2011). Collectively, these results do not point to a clear mechanism for the large intermodel spread in the mean-state AMOC strength across coupled GCMs.

Variations in the AMOC strength can also be related to interior processes through thermal-wind balance, which links meridional density gradients to meridional volume transport under an assumption of mass conservation between zonal and meridional volume transport. Building on earlier efforts (e.g., Robinson & Stommel, 1959; Bryan, 1987; Marotzke, 1997), a series of recent studies have shown that the thermal-wind expression can approximate the AMOC strength in more comprehensive ocean-only and coupled GCMs (Gnanadesikan, 1999; De Boer et al., 2010; Jansen et al., 2018; Sigmond et al., 2020; Waldman et al., 2021; Bonan et al., 2022). However, it is unclear which aspect of the thermal-wind balance contributes to the intermodel spread in AMOC strength in coupled GCMs. Does the meridional density difference or overturning scale depth contribute more to the intermodel spread in AMOC strength? Furthermore, it is unclear how to relate the circulation implied by the thermal-wind expression to the circulation implied by surface water mass transformation, which must be equivalent in steady state. Indeed, previous studies have introduced conceptual frameworks that link surface water mass transformation to the interior overturning circulation (e.g., Spall, 2004; Straneo, 2006b, 2006a; Spall, 2011, 2012), but these studies used idealized models and focused on more regional domains, such as the marginal Arctic seas. A framework relating surface processes to the basin-scale overturning circulation in coupled GCMs is lacking, and thus, our understanding of how surface and interior ocean processes relate to the intermodel spread in mean-state AMOC strength remains unclear.

In this study, we introduce a framework for understanding the intermodel spread in the mean-state AMOC strength in coupled GCMs by linking the thermal-wind expression to surface water mass transformation in the North Atlantic. In what follows, we first describe the CMIP6 output and the thermal-wind expression. We then show that the thermal-wind expression emulates the strength of the AMOC in coupled GCMs. We find that the intermodel spread in the mean-state AMOC strength is dominated by the intermodel spread in the overturning scale depth. We further find that the overturning scale depth can be related to North Atlantic surface buoyancy fluxes and stratification. GCMs with a deeper scale depth tend to have stronger North Atlantic surface buoyancy loss and weaker North Atlantic stratification. These results provide a pathway for reducing biases in the mean-state AMOC across GCMs.

2 Data and Methods

2.1 CMIP6 output

This study uses monthly output from 22 pre-industrial control (piControl) simulations for GCMs participating in CMIP6 (see Figure 1 for climate model names). Each simulation is from the r1i1p1f1 variant label. The model output is averaged over the last 200 years of each simulation.

The AMOC strength is defined as the maximum value of the meridional overturning streamfunction (msftmz and msftmy) in the Atlantic basin poleward of 30°N and below 500 m. The parentheses denote CMIP6 variable names. The choice of 500 m avoids volume flux contributions associated with the subtropical ocean gyres. The surface buoyancy flux (discussed in more detail below), is computed using the net surface heat flux (hfds) and net surface freshwater flux (wfo). Finally, ocean potential density referenced to 1000 dbar is calculated from ocean potential temperature (thetao) and ocean absolute salinity (so).

2.2 Surface buoyancy flux

The surface buoyancy flux F_b (units of m^2 s^{-3}) is calculated using a linear equation of state:

$$F_b = \underbrace{\frac{g\alpha}{\rho_0 c_p} Q_s}_{\text{thermal}} + \underbrace{g\beta S_0 F_s}_{\text{haline}}, \tag{1}$$

where g is the gravitational acceleration (9.81 m s^{-2}), ρ_0 is a reference density of seawater (1027.5 kg m^{-3}), c_p is the heat capacity of seawater (4000 J kg^{-1} K^{-1}), α is the thermal expansion coefficient (-1.5×10^{-4} K^{-1}), β is the haline contraction coefficient (7.6×10^{-4} kg g^{-1}), and S_0 is reference salinity (35 g kg^{-1}). Here, Q_s is the net surface heat flux (in W m^{-2}) and represents the thermal component, and F_s is the net surface freshwater flux (in m s^{-1}) and represents the haline component. Both are defined as positive downwards meaning positive for ocean heat gain and ocean freshwater gain. Note that the results described below are similar whether α and β are constant or spatially varying (not shown).

3 Controls on the AMOC in CMIP6

We begin by applying the thermal-wind expression to each CMIP6 piControl simulation. Previous studies have shown that the thermal-wind expression, which links the strength of the overturning circulation to the density contrast between the northern sinking region and more southern latitudes, provides a good approximation of the AMOC strength in GCMs (De Boer et al., 2010; Jansen et al., 2018; Johnson et al., 2019; Sigmond et al., 2020; Bonan et al., 2022). The interior overturning circulation ψ_{int} implied by the thermal-wind expression is given by

$$\psi_{\text{int}} = \frac{g}{2\rho_0 f_0} \Delta_y \rho H^2, \tag{2}$$

where f_0 is the Coriolis parameter (1×10^{-4} s^{-1}), $\Delta_y \rho$ is the meridional density difference between the North Atlantic and low-latitude Atlantic (kg m^{-3}), and H is the scale depth (m). Note that ψ_{int} represents the "interior" volume transport and is distinct from the surface volume transport arising from surface water mass transformation (which is discussed in Section 3.2).

Following De Boer et al. (2010), $\Delta_y \rho$ is calculated as the vertical average of the difference in potential density between the North Atlantic (area-averaged from 40°N to 60°N) and the low-latitude Atlantic (area-averaged from 30°S to 30°N) over the upper 1000 meters of the Atlantic basin. This accounts for density variations in the upper cell. H is calculated as the depth where the depth-integrated $\Delta_y \rho(z)$ (for the same regional domains) equals the vertical mean of the depth-integrated $\Delta_y \rho(z)$. In other words, H is calculated as

$$\int_{-H}^{0} \Delta_y \rho(z) \ dz = \frac{1}{D} \int_{-D}^{0} \Delta_y \rho(z) z \ dz, \tag{3}$$

where D is the depth of the entire water column. This estimate of H is approximately the depth of maximum zonal volume transport (De Boer et al., 2010).

The thermal-wind expression (Eq. 2) emulates the AMOC strength in each GCM, accounting for approximately 84% of the intermodel variance and having a root-mean-square error of approximately 2 Sv (Fig. 2a). The strong agreement between the AMOC strength and thermal-wind expression in each GCM suggests that intermodel differences in the AMOC strength can be attributed to intermodel differences in $\Delta_y \rho$ and H (Fig. 2b).

3.1 Controls on the AMOC strength

Based on the success of the thermal-wind expression in approximating the AMOC strength in GCMs, we perform a perturbation analysis of $\Delta_y \rho$ and H to explore which term contributes most to the intermodel spread in the AMOC strength. Defining the multi-model mean as $\overline{(\cdot)}$

and deviations from the multi-model mean (the intermodel spread) as $(\cdot)'$, the intermodel spread can be decomposed as

$$\psi'_{\text{int}} = \frac{g}{2\rho_0 f_0} \left(\underbrace{\Delta_y \rho' \overline{H}^2}_{(1)} + \underbrace{\overline{\Delta_y \rho} 2\overline{H} H'}_{(2)} + \underbrace{\epsilon}_{(3)} \right), \tag{4}$$

where (1) represents intermodel variations in the AMOC strength due to intermodel variations in $\Delta_y \rho$; (2) represents intermodel variations in the AMOC strength due to intermodel variations in H; and (3) represents higher order residual terms.

The intermodel spread in the AMOC strength is more strongly dependent on the intermodel spread in H, with $\Delta_y \rho$ playing a secondary role (compare green and orange bars in Fig. 2c). The residual terms contribute little to the intermodel spread of the AMOC strength (see grey bars in Fig. 2c). Intermodel variations in H account for approximately 76% of the intermodel variance in AMOC strength (green bars, Fig. 2c), whereas intermodel variations in $\Delta_y \rho$ account for approximately 31% of the intermodel variance (orange bars, Fig. 2c). Note, however, that H and $\Delta_y \rho$ are somewhat correlated (De Boer et al., 2010) and therefore are not entirely independent of each other. Still, intermodel variations in H have an outsized importance, most evident in GCMs with extremely weak or strong AMOC strengths. For example, GCMs that exhibit the weakest mean-state AMOC strength (IPSL-CM6A-LR, CanESM5, UKESM1-0-LL) tend to have the smallest H, while GCMs that exhibit the strongest mean-state AMOC strength (NorESM2-MM, NorESM2-LM, MPI-ESM1-2-LR) tend to have the largest H.

Physically, these results show that a stronger AMOC is linked to a stronger meridional density gradient. However, differences in the AMOC strength across GCMs are primarily driven by differences in the overturning scale depth (Fig. 2c), which is related to the spatial distribution of outcropping density classes in the North Atlantic, rather than the total difference in density between low- and high-latitude water masses.

3.2 Connection to North Atlantic processes

The strong control of H on the mean-state AMOC strength in GCMs suggests a fundamental relationship between H and surface processes in the North Atlantic. In steady-state, the interior overturning circulation ψ_{int} implied by the thermal-wind expression must balance the volume transport associated with the surface water mass transformation, assuming interior diabatic processes are relatively small. Previous studies have related surface water mass transformation to the interior circulation of the marginal Arctic seas (e.g., Spall, 2004), but have not related surface water mass transformation to the basin-wide overturning circulation. Building on earlier work by Speer and Tziperman (1992) and motivated by application of residual mean theory to the surface buoyancy budget in the Southern Ocean (Marshall & Radko, 2003), we expect the North Atlantic overturning transport in the surface mixed layer ψ_{sfc} to depend on the magnitude of the surface buoyancy flux F_b and the surface meridional buoyancy gradient $\partial b/\partial y$, such that

$$\psi_{\text{sfc}} = \frac{F_b}{\partial b/\partial y} L_x, \tag{5}$$

where L_x is a zonal width scale that represents the zonal distance of the basin (see Eq. (11) in Marshall and Radko (2003)). However, because the region of surface water mass transformation in the North Atlantic varies widely across GCMs (e.g., Jackson & Petit, 2023), we modify this relationship to express ψ_{sfc} in terms of the vertical stratification N^2 of the North Atlantic

$$N^2 \equiv -\frac{g}{\rho_0} \frac{\partial \rho}{\partial z}, \tag{6}$$

and the isopycnal slope S of the North Atlantic

$$S \equiv -\frac{\partial b/\partial y}{\partial b/\partial z} \approx \frac{H}{L_y}, \tag{7}$$

where L_y is a meridional length scale that represents the meridional distance over which interior isopycnals tilt up towards their surface outcrop location. In other words, to alleviate concerns about the location of $\partial b/\partial y$ in each GCM, we estimate $\partial b/\partial y$ from a bulk average of interior ocean processes (i.e., $\partial b/\partial y \approx N^2 S$). This results in the relationship

$$\psi_{\text{sfc}} = \frac{F_b}{N^2}\frac{L_x}{S}. \tag{8}$$

This relationship assumes the interior isopycnals that outcrop in the North Atlantic are geometrically confined due to land masses, such that L_y is constant.

Assuming steady-state conditions and that interior diabatic processes in the AMOC density classes are negligible, Eqs. (2) and (8) can be combined to relate H in terms of North Atlantic properties,

$$H = \left(\frac{F_b}{N^2}\frac{L_x L_y}{\Delta_y \rho}\frac{2\rho_0 f_0}{g} \right)^{1/3}. \tag{9}$$

Eq. (9) shows that $H \sim F_b^{1/3}$, and $H \sim N^2, \Delta_y \rho^{-1/3}$. Eq. (9) shares a similar form to other scalings for H (Gnanadesikan, 1999; Klinger & Marotzke, 1999; Marotzke & Klinger, 2000; Youngs et al., 2020). For example, Klinger and Marotzke (1999) found a power of $1/3$ dependence on H but instead related H to the vertical diffusivity of the interior ocean. Eq. (9) describes the sensitivity of H to North Atlantic processes, specifically the magnitude of the North Atlantic stratification and surface buoyancy flux, rather than interior ocean or Southern Ocean processes. A stronger F_b or weaker N^2 is associated with a deeper H.

The surface buoyancy flux F_b is area-averaged in the region of water mass transformation (40°N to 70°N in the Atlantic basin). The vertical stratification N^2 is estimated as the area-averaged value for the same regional domain and further averaged over the upper 1000 m. Here, we exclude the upper 0–100 m, which represents the ocean's surface mixed layer. Our results are not sensitive to precise mixed layer depth so long as the depth captures where interior isopycnals outcrop into the surface mixed layer. Thus, this estimation captures variations in stratification associated with outcropping isopycnals. L_x is assumed to be 10000 km for all GCMs, and represents a crude approximations of the zonal width of the Atlantic basin. L_y is assumed to be 3000 km for all GCMs.

Figure 3a shows a comparison of H (black bars) diagnosed from GCMs and H (black hatched bars) predicted from Eq. (9). This expression accounts for approximately 65% of the intermodel variance in H and tends to accurately predict values of H for GCMs with a variety of AMOC strengths (Fig. 3a). Note that Eq. (9) generally underpredicts the magnitude of H in most GCMs, likely because of our choices of L_x and L_y.

Isolating the intermodel spread in F_b, N^2, and $\Delta_y \rho$ by fixing two variables as the multi-model mean and applying the intermodel spread of the other variable, allows us to understand how the intermodel spread in North Atlantic processes relate to the intermodel spread in H. Intermodel variations in F_b and N^2 dominate the intermodel spread in H, accounting for approximately 40% and 60% of the intermodel variance. $\Delta_y \rho$ contributes very little to the intermodel variance in H (Fig. 3b).

4 Discussion and conclusions

Coupled GCMs exhibit a large intermodel spread in the mean-state AMOC, with strengths varying between 12 and 25 Sv (Fig. 1). In this study, we introduce a framework for understanding the intermodel spread in the AMOC strength across GCMs by assessing the thermal-wind expression and surface water mass transformation.

We find that the intermodel spread in the AMOC strength can be approximated by the thermal-wind expression (Eq. 2). These results build on earlier work by De Boer et al. (2010), which showed that the thermal-wind expression provides a good approximation to the AMOC strength in ocean-only GCMs. Here, we show that the thermal-wind expression provides a good approximation the AMOC strength in coupled GCMs. We also show that intermodel variations in H contribute most to intermodel variations in the AMOC strength (Fig. 2). GCMs with a deeper H tend to have a stronger AMOC. We further link H to North Atlantic surface water mass transformation (Eq. 9 and Fig. 3) and find that GCMs with a deeper H tend to also have stronger surface buoyancy loss and weaker stratification in the North Atlantic.

Together the thermal wind and surface water mass transformation frameworks allow us to summarize the AMOC strength in GCMs as a function of several key ocean features (Figure 4). Specifically, we show that the intermodel spread in the Atlantic basin meridional density difference $\Delta_y\rho$ contributes little to the intermodel spread in AMOC strength across GCMs. Thus, GCMs with strong $\Delta_y\rho$ (Fig. 4a) or weak $\Delta_y\rho$ (Fig. 4b), as indicated by the difference in color between each density class and the orange arrows, exhibit little variation in the mean-state AMOC strength. Instead, the intermodel spread in the AMOC strength across GCMs is related to the intermodel spread in the overturning scale depth H. GCMs with a weak mean-state AMOC generally exhibit a shallower H (Fig. 4c), while GCMs with a strong mean-state AMOC generally exhibit a deeper H (Fig. 4d). We also show that GCMs with a deeper H exhibit more North Atlantic surface buoyancy loss (indicated by the blue arrows) and weaker North Atlantic stratification (indicated by the grey lines). In fact, intermodel variations in North Atlantic surface buoyancy loss and stratification account for approximately 40% and 60% of the intermodel variance in H, respectively. However, because we examined steady-state simulations, the causality is unclear. Future work should examine whether a deeper H leads to a stronger AMOC and thus more surface buoyancy loss and weaker stratification in the North Atlantic, or if stronger surface buoyancy loss leads to weaker stratification, a deeper H, and a stronger AMOC.

A key implication of this work is that constraining the intermodel spread in H may ultimately constrain the intermodel spread in the AMOC strength across GCMs. Here, we introduced a perspective that details North Atlantic controls on the depth of H, by linking North Atlantic surface buoyancy loss and stratification to H (Eq. 9). Our results imply that reducing the intermodel spread in North Atlantic surface buoyancy loss could reduce the intermodel spread in H and, therefore, the AMOC strength. For example, better representing shortwave and longwave cloud radiative fluxes or surface winds over the North Atlantic might improve modeled North Atlantic surface buoyancy loss and reduce the intermodel spread in H and thus the AMOC strength.

However, other studies show that H depends strongly on interior ocean processes, such as vertical diffusivity (Klinger & Marotzke, 1999; Marotzke & Klinger, 2000; Nikurashin & Vallis, 2012), or on Southern Ocean processes, such as Ekman and eddy transport (Toggweiler & Samuels, 1998; Gnanadesikan, 1999; Nikurashin & Vallis, 2012; Thompson et al., 2016; Marshall et al., 2017; Nadeau & Jansen, 2020; Baker et al., 2021), which implies other sources of intermodel spread in H. Additionally, recent work has argued that remote low-latitude processes can also play an important role in setting the Atlantic basin stratification and thus H (e.g., Newsom & Thompson, 2018; Cessi, 2019; Newsom et al., 2021; Baker et al., 2021), which implies that H may also be controlled by inter-basin ocean dynamics (Thompson et al., 2016; Nadeau & Jansen, 2020). However, it is thus far unclear how to reconcile the nonlocal perspective on H with the local, North Atlantic perspective introduced in this study.

Constraining the intermodel spread in H may also help to constrain the climate response to greenhouse-gas forcing. Several studies have shown a clear link between the depth of the AMOC and the depth of ocean heat storage under warming (Kostov et al., 2014; Saenko et al., 2018; Gregory et al., 2023). While these studies largely attribute this link to Southern

Ocean processes (Kuhlbrodt & Gregory, 2012; Saenko et al., 2018; Newsom et al., 2023), it suggests that constraining H might constrain the the transient climate response. Furthermore, numerous studies have shown that the mean-state AMOC strength is related to AMOC weakening under warming, implying that, regardless of the mechanisms setting the contemporary AMOC strength, this strength may be predictive of future AMOC declines (Gregory et al., 2005; Weaver et al., 2012; Winton et al., 2014; Weijer et al., 2020; Bonan et al., 2022; Baker et al., 2023). Thus, our work implies that improving mean-state processes that impact H, whether it be locally in the North Atlantic or non-locally in the Southern and Indo-Pacific Oceans, will ultimately lead to a better understanding of how the AMOC changes under warming.
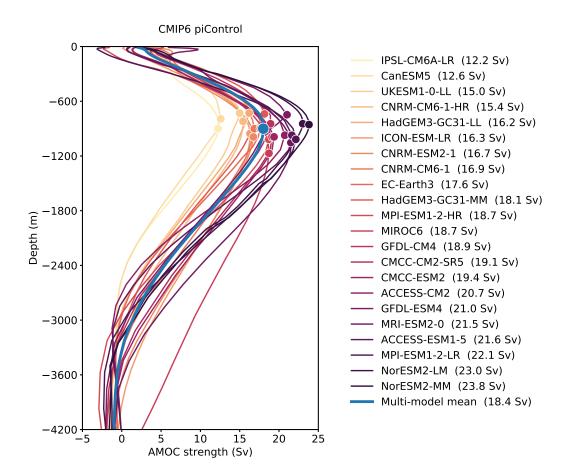
Figure 1. **The mean-state AMOC in CMIP6 climate models.** Profile of the meridional overturning streamfunction in the Atlantic basin at the latitude of maximum AMOC strength (poleward of 30°N) for each CMIP6 piControl simulation. The circle markers denote the maximum AMOC strength for each GCM. The maximum AMOC strength is also listed next to each climate model name in the legend. Climate models are listed and color coded from weakest-to-strongest mean-state AMOC strength. The blue line is the multi-model mean AMOC.
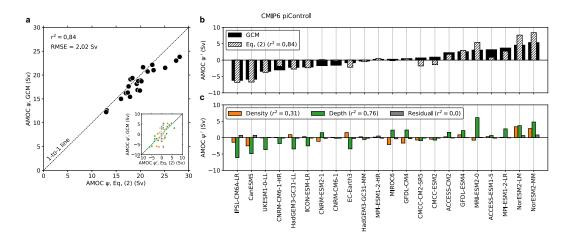
Figure 2. Controls on the AMOC strength. (a) Scatter plot of the AMOC strength predicted by the thermal-wind expression (Eq. 2) versus the AMOC strength diagnosed from the climate models. (b) Bar plot showing the intermodel spread in the AMOC strength (solid black) diagnosed from the climate models and (hatch black) predicted by the thermal-wind expression (Eq. 2). (c) Bar plot showing the contribution of the three terms in Eq. (4) to the intermodel spread in the AMOC strength. Climate models are ordered from weakest-to-strongest mean-state AMOC strength for (b) and (c). The proportion of variance explained is in the legend of each sub-panel. Panel (a) contains an inset figure that shows visually how each term in Eq. (4) contributes to the intermodel spread in the AMOC strength.
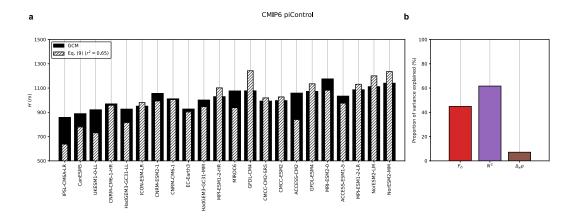
Figure 3. **Connection between the overturning scale depth H and the North Atlantic.** (a) Bar plot showing (solid black) H diagnosed from the climate models and (hatch black) H predicted by Eq. (9). Climate models are ordered from weakest-to-strongest mean-state AMOC strength. (b) Bar plot showing the proportion of variance explained by the intermodel variance in (red) North Atlantic surface buoyancy loss F_b, (purple) North Atlantic stratification N^2, and (brown) the meridional density difference in the Atlantic basin $\Delta_y \rho$.

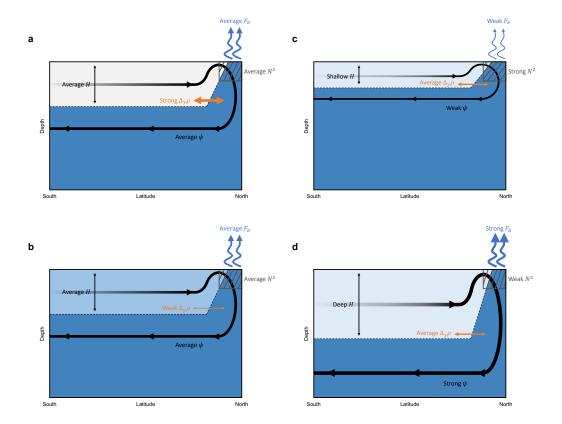**Figure 4. Schematic describing controls on the AMOC in CMIP6.** A schematic describing the processes in climate models that are associated with a weak mean-state AMOC and a strong mean-state AMOC. The dashed line denotes the overturning scale depth (H). The streamline denotes the AMOC strength (ψ). The blue arrows denote surface buoyancy loss in the North Atlantic (F_b). In each grey box, the grey lines are parallel to the slope of the isopycnal. Steeper isopycnals denote weaker North Atlantic stratification (N^2). The orange arrow and colors of each density layer denotes the meridional density difference ($\Delta_y \rho$). Climate models with (a) stronger or (b) weaker $\Delta_y \rho$ tend to have similar AMOC strengths. However, climate models with a (c) shallower or (d) deeper H tend to have a weaker or a stronger AMOC, weaker or stronger F_b, and stronger or weaker N^2, respectively.

Acknowledgments

Open Research

The authors thank the climate modeling groups for producing and making available their model output, which is accessible at the Earth System Grid Federation (ESGF) Portal (https://esgf-node.llnl.gov/search/cmip6/). A list of the CMIP6 models used in this study is provided in Figure 1 and described in Section 2.1.

References

Abernathey, R., Marshall, J., & Ferreira, D. (2011, 12). The dependence of southern ocean meridional overturning on wind stress. *Journal of Physical Oceanography*, *41*, 2261-2278. doi: 10.1175/JPO-D-11-023.1

Baker, J. A., Bell, M. J., Jackson, L. C., Renshaw, R., Vallis, G. K., Watson, A. J., & Wood, R. A. (2023). Overturning pathways control AMOC weakening in CMIP6 models. *Geophysical Research Letters*, *50*(14), e2023GL103381.

Baker, J. A., Watson, A. J., & Vallis, G. K. (2020). Meridional overturning circulation in a multibasin model. Part I: dependence on Southern Ocean buoyancy forcing. *Journal of Physical Oceanography*, *50*(5), 1159–1178.

Baker, J. A., Watson, A. J., & Vallis, G. K. (2021). Meridional overturning circulation in a multibasin model. part ii: Sensitivity to diffusivity and wind in warm and cool climates. *Journal of Physical Oceanography*, *51*(6), 1813–1828.

Bonan, D. B., Thompson, A. F., Newsom, E. R., Sun, S., & Rugenstein, M. (2022). Transient and equilibrium responses of the Atlantic overturning circulation to warming in coupled climate models: the role of temperature and salinity. *Journal of Climate*, *35*(15), 5173–5193.

Broecker, W. S. (1991). The great ocean conveyor. *Oceanography*, *4*(2), 79–89.

Bryan, F. (1987). Parameter sensitivity of primitive equation ocean general circulation models. *Journal of Physical Oceanography*, *17*(7), 970–985.

Buckley, M. W., & Marshall, J. (2016). Observations, inferences, and mechanisms of the Atlantic Meridional Overturning Circulation: A review. *Reviews of Geophysics*, *54*(1), 5-63.

Cessi, P. (2019). The Global Overturning Circulation. *Annual Review of Marine Science*, *11*(1), 249-270.

Cheng, W., Chiang, J. C. H., & Zhang, D. (2013). Atlantic meridional overturning circulation (amoc) in cmip5 models: Rcp and historical simulations. *Journal of Climate*, *26*(18), 7187 - 7197.

De Boer, A. M., Gnanadesikan, A., Edwards, N. R., & Watson, A. J. (2010). Meridional density gradients do not control the Atlantic overturning circulation. *Journal of Physical Oceanography*, *40*(2), 368–380.

Ferrari, R., Jansen, M. F., Adkins, J. F., Burke, A., Stewart, A. L., & Thompson, A. F. (2014). Antarctic sea ice control on ocean circulation in present and glacial climates. *Proceedings of the National Academy of Sciences*, *111*(24), 8753–8758.

Frierson, D. M., Hwang, Y.-T., Fučkar, N. S., Seager, R., Kang, S. M., Donohoe, A., ... Battisti, D. S. (2013). Contribution of ocean overturning circulation to tropical rainfall peak in the Northern Hemisphere. *Nature Geoscience*, *6*(11), 940–944.

Ganachaud, A., & Wunsch, C. (2003). Large-scale ocean heat and freshwater transports during the world ocean circulation experiment. *Journal of Climate*, *16*(4), 696 - 705.

Gent, P. R. (2016). Effects of southern hemisphere wind changes on the meridional overturning circulation in ocean models. *Annual review of marine science*, *8*, 79–94.

Gnanadesikan, A. (1999, 04). A Simple Predictive Model for the Structure of the Oceanic Pycnocline. *Science (New York, N.Y.)*, *283*, 2077-9. doi: 10.1126/science.283.5410.2077

Gordon, A. L. (1986). Interocean exchange of thermocline water. *Journal of Geophysical Research: Oceans*, *91*(C4), 5037–5046.

Gregory, J. M., Bloch-Johnson, J., Couldrey, M. P., Exarchou, E., Griffies, S. M., Kuhlbrodt, T., ... Zanna, L. (2023). *A new conceptual model of global ocean heat uptake* (No. 0123456789). Springer Berlin Heidelberg. doi: 10.1007/s00382-023-06989-z

Gregory, J. M., Dixon, K. W., Stouffer, R. J., Weaver, A. J., Driesschaert, E., Eby, M., ... others (2005). A model intercomparison of changes in the Atlantic thermohaline circulation in response to increasing atmospheric CO2 concentration. *Geophysical Research Letters*, *32*(12).

Heuzé, C. (2021). Antarctic bottom water and North Atlantic deep water in CMIP6 models. *Ocean Science*, *17*(1), 59–90.

Hughes, T. M. C., & Weaver, A. J. (1994). Multiple equilibria of an asymmetric two-basin ocean model. *Journal of Physical Oceanography*, *24*(3), 619 - 637.

Jackson, L., & Petit, T. (2023). North Atlantic overturning and water mass transformation in CMIP6 models. *Climate Dynamics*, *60*(9-10), 2871–2891.

Jansen, M. F., & Nadeau, L.-P. (2016). The effect of Southern Ocean surface buoyancy loss on the deep-ocean circulation and stratification. *Journal of Physical Oceanography*, *46*(11), 3455–3470.

Jansen, M. F., Nadeau, L.-P., & Merlis, T. M. (2018). Transient versus equilibrium response of the ocean's overturning circulation to warming. *Journal of Climate*, *31*(13), 5147–5163.

Jochum, M., & Eden, C. (2015). The connection between Southern Ocean winds, the Atlantic meridional overturning circulation, and Indo-Pacific upwelling. *Journal of Climate*, *28*(23), 9250–9257.

Johnson, H. L., Cessi, P., Marshall, D. P., Schloesser, F., & Spall, M. A. (2019). Recent contributions of theory to our understanding of the atlantic meridional overturning circulation. *Journal of Geophysical Research: Oceans*, *124*(8), 5376-5399.

Klinger, B. A., & Marotzke, J. (1999). Behavior of double-hemisphere thermohaline flows in a single basin. *Journal of physical oceanography*, *29*(3), 382–399.

Kostov, Y., Armour, K. C., & Marshall, J. (2014). Impact of the Atlantic Meridional Overturning Circulation on Ocean Heat Storage and Transient Climate Change. *Geophysical Research Letters*.

Kuhlbrodt, T., & Gregory, J. M. (2012). Ocean heat uptake and its consequences for the magnitude of sea level rise and climate change. *Geophysical Research Letters*, *39*(17), 1–6. doi: 10.1029/2012GL052952

Lin, Y.-J., Rose, B. E., & Hwang, Y.-T. (2023). Mean state AMOC affects AMOC weakening through subsurface warming in the Labrador Sea. *Journal of Climate*, *36*(12), 3895–3915.

Lumpkin, R., & Speer, K. (2007). Global ocean meridional overturning. *Journal of Physical Oceanography*, *37*(10), 2550–2562.

Mahajan, S., Zhang, R., & Delworth, T. L. (2011). Impact of the Atlantic meridional overturning circulation (AMOC) on Arctic surface air temperature and sea ice variability. *Journal of Climate*, *24*(24), 6573–6581.

Marotzke, J. (1997). Boundary mixing and the dynamics of three-dimensional thermohaline circulations. *Journal of Physical Oceanography*, *27*(8), 1713–1728.

Marotzke, J., & Klinger, B. A. (2000). The dynamics of equatorially asymmetric thermohaline circulations. *Journal of physical oceanography*, *30*(5), 955–970.

Marshall, J., Donohoe, A., Ferreira, D., & McGee, D. (2014). The ocean's role in setting

the mean position of the Inter-Tropical Convergence Zone. *Climate Dynamics*, *42*, 1967–1979.

Marshall, J., & Radko, T. (2003). Residual-mean solutions for the Antarctic Circumpolar Current and its associated overturning circulation. *Journal of Physical Oceanography*, *33*(11), 2341–2354.

Marshall, J., Scott, J. R., Romanou, A., Kelley, M., & Leboissetier, A. (2017). The dependence of the ocean's MOC on mesoscale eddy diffusivities: A model study. *Ocean Modelling*, *111*, 1–8. Retrieved from `http://dx.doi.org/10.1016/j.ocemod.2017.01.001` doi: 10.1016/j.ocemod.2017.01.001

Nadeau, L.-P., & Jansen, M. F. (2020). Overturning circulation pathways in a two-basin ocean model. *Journal of Physical Oceanography*, *50*(8), 2105–2122.

Newsom, E. R., & Thompson, A. F. (2018). Reassessing the role of the Indo-Pacific in the ocean's global overturning circulation. *Geophysical Research Letters*, *45*(22), 12–422.

Newsom, E. R., Thompson, A. F., Adkins, J. F., & Galbraith, E. D. (2021). A hemispheric asymmetry in poleward ocean heat transport across climates: Implications for overturning and polar warming. *Earth and Planetary Science Letters*, *568*, 117033.

Newsom, E. R., Zanna, L., & Gregory, J. M. (2023). Background Pycnocline Depth Constrains Future Ocean Heat Uptake Efficiency. *Geophysical Research Letters*, *50*(22), 1–11. doi: 10.1029/2023GL105673

Nikurashin, M., & Vallis, G. (2012). A theory of the interhemispheric meridional overturning circulation and associated stratification. *Journal of Physical Oceanography*, *42*(10), 1652–1667.

Radko, T., & Kamenkovich, I. (2011). Semi-adiabatic model of the deep stratification and meridional overturning. *Journal of physical oceanography*, *41*(4), 757–780.

Reintges, A., Martin, T., Latif, M., & Keenlyside, N. S. (2017). Uncertainty in twenty-first century projections of the Atlantic Meridional Overturning Circulation in CMIP3 and CMIP5 models. *Climate Dynamics*, *49*, 1495–1511.

Robinson, A., & Stommel, H. (1959). The oceanic thermocline and the associated thermohaline circulation 1. *Tellus*, *11*(3), 295–308.

Saenko, O. A., Yang, D., & Gregory, J. M. (2018). Impact of mesoscale eddy transfer on heat uptake in an eddy-parameterizing ocean model. *Journal of Climate*, *31*(20), 8589–8606. doi: 10.1175/JCLI-D-18-0186.1

Samelson, R. (2009). A simple dynamical model of the warm-water branch of the middepth meridional overturning cell. *Journal of physical oceanography*, *39*(5), 1216–1230.

Schmittner, A., Latif, M., & Schneider, B. (2005). Model projections of the North Atlantic thermohaline circulation for the 21st century assessed by observations. *Geophysical research letters*, *32*(23).

Sévellec, F., & Fedorov, A. V. (2011). Stability of the Atlantic meridional overturning circulation and stratification in a zonally averaged ocean model: Effects of freshwater flux, Southern Ocean winds, and diapycnal diffusion. *Deep Sea Research Part II: Topical Studies in Oceanography*, *58*(17-18), 1927–1943.

Sévellec, F., & Fedorov, A. V. (2016). AMOC sensitivity to surface buoyancy fluxes: Stronger ocean meridional heat transport with a weaker volume transport? *Climate Dynamics*, *47*(5-6), 1497–1513.

Shakespeare, C. J., & Hogg, A. M. (2012). An analytical model of the response of the meridional overturning circulation to changes in wind and buoyancy forcing. *Journal of Physical Oceanography*, *42*(8), 1270 - 1287. Retrieved from `https://journals.ametsoc.org/view/journals/phoc/42/8/jpo-d-11-0198.1.xml` doi: https://doi.org/10.1175/JPO-D-11-0198.1

Sigmond, M., Fyfe, J. C., Saenko, O. A., & Swart, N. C. (2020). Ongoing AMOC and related sea-level and temperature changes after achieving the Paris targets. *Nature Climate Change*, *10*(7), 672–677.

Spall, M. A. (2004). Boundary currents and watermass transformation in marginal seas. *Journal of physical oceanography*, *34*(5), 1197–1213.

Spall, M. A. (2011). On the role of eddies and surface forcing in the heat transport and overturning circulation in marginal seas. *Journal of Climate*, *24*(18), 4844–4858.

Spall, M. A. (2012). Influences of precipitation on water mass transformation and deep convection. *Journal of physical oceanography*, *42*(10), 1684–1700.

Speer, K., & Tziperman, E. (1992). Rates of water mass formation in the North Atlantic Ocean. *Journal of Physical Oceanography*, *22*(1), 93–104.

Stommel, H. (1961). Thermohaline convection with two stable regimes of flow. *Tellus*, *13*(2), 224-230.

Straneo, F. (2006a). Heat and freshwater transport through the central labrador sea. *Journal of Physical Oceanography*, *36*(4), 606–628.

Straneo, F. (2006b). On the connection between dense water formation, overturning, and poleward heat transport in a convective basin. *Journal of Physical Oceanography*, *36*(9), 1822–1840.

Talley, L. D. (2013). Closure of the global overturning circulation through the Indian, Pacific, and Southern Oceans: Schematics and transports. *Oceanography*, *26*(1), 80–97.

Thompson, A. F., Stewart, A. L., & Bischoff, T. (2016). A multibasin residual-mean model for the global overturning circulation. *Journal of Physical Oceanography*, *46*(9).

Thorpe, R. B., Gregory, J. M., Johns, T. C., Wood, R. A., & Mitchell, J. F. B. (2001). Mechanisms determining the atlantic thermohaline circulation response to greenhouse gas forcing in a non-flux-adjusted coupled climate model. *Journal of Climate*, *14*(14), 3102 - 3116.

Toggweiler, J., & Samuels, B. (1998). On the ocean's large-scale circulation near the limit of no vertical mixing. *Journal of Physical Oceanography*, *28*(9), 1832–1852.

Vallis, G. K. (2000). Large-scale circulation and production of stratification: Effects of wind, geometry, and diffusion. *Journal of Physical Oceanography*, *30*(5), 933–954.

Waldman, R., Hirschi, J., Voldoire, A., Cassou, C., & Msadek, R. (2021). Clarifying the relation between AMOC and thermal wind: Application to the centennial variability in a coupled climate model. *Journal of Physical Oceanography*, *51*(2), 343–364.

Wang, C., Dong, S., & Munoz, E. (2010). Seawater density variations in the North Atlantic and the Atlantic meridional overturning circulation. *Climate dynamics*, *34*, 953–968.

Weaver, A. J., Sedláček, J., Eby, M., Alexander, K., Crespin, E., Fichefet, T., . . . others (2012). Stability of the Atlantic meridional overturning circulation: A model intercomparison. *Geophysical Research Letters*, *39*(20).

Weijer, W., Cheng, W., Garuba, O. A., Hu, A., & Nadiga, B. T. (2020). CMIP6 Models Predict Significant 21st Century Decline of the Atlantic Meridional Overturning Circulation. *Geophysical Research Letters*, *47*(12), e2019GL086075.

Winton, M., Anderson, W. G., Delworth, T. L., Griffies, S. M., Hurlin, W. J., & Rosati, A. (2014). Has coarse ocean resolution biased simulations of transient climate sensitivity? *Geophysical Research Letters*, *41*(23), 8522–8529.

Wolfe, C. L., & Cessi, P. (2010). What sets the strength of the middepth stratification and overturning circulation in eddying ocean models? *Journal of Physical Oceanography*, *40*(7), 1520–1538.

Wolfe, C. L., & Cessi, P. (2011). The adiabatic pole-to-pole overturning circulation. *Journal of Physical Oceanography*, *41*(9), 1795–1810.

Youngs, M. K., Ferrari, R., & Flierl, G. R. (2020). Basin-width dependence of northern deep convection. *Geophysical Research Letters*, *47*(15), e2020GL089135.

Zhang, R., & Delworth, T. L. (2006). Impact of Atlantic multidecadal oscillations on India/Sahel rainfall and Atlantic hurricanes. *Geophysical research letters*, *33*(17).

Zhang, R., Sutton, R., Danabasoglu, G., Kwon, Y.-O., Marsh, R., Yeager, S. G., . . . Little, C. M. (2019). A review of the role of the Atlantic meridional overturning circulation in Atlantic multidecadal variability and associated climate impacts. *Reviews of Geophysics*, *57*(2), 316–375.